Laser and Particle Beams (2012), *30*, 665–670.

doi:10.1017/S0263034612000638

X-ray emission induced by 1.2–3.6 MeV Kr^{13+} ions

CEXIANG MEI,[1,2] YONGTAO ZHAO,[3] XIAOAN ZHANG,[2] JIERU REN,[3] XIANMING ZHOU,[3] XING WANG,[3] YU LIE,[3] CHANGHUI LIANG,[2] YAOZONG LI,[2] AND GUOQING XIAO[3]

[1]Department of Applied Physics, Xi'an Jiaotong University, Xi'an, China
[2]School of Physics and Electronic Engineering, Xianyang Normal University, Xianyang, China
[3]Institute of Modern Physics, Chinese Academy of Science, Lanzhou, China

(RECEIVED 16 July 2012; ACCEPTED 25 July 2012)

Abstract

X-ray emission from Kr^{13+} ions in the energy range 1.2–3.6 MeV in steps of 0.6 MeV impacting on an Au target was investigated on electron cyclotron resonance ion source at the Heavy Ion Research Facility in Lanzhou. It was found that a shift of the X-ray lines to the higher energy side occurred. We measured the relationship between the characteristic of X-ray yield of Au M X-rays and Kr L X-rays as a function of incident energy. Furthermore, M-shell X-ray production cross-section of Au induced by Kr^{13+} was measured. The measured cross-section of target is compared to the classical binary-encounter approximation and plane-wave-born approximation theoretical model, which is a significant different between experimental and theoretical model.

Keywords: Energy shift and line broadening; Inertial X-ray; Ion beam matter interaction

1. INTRODUCTION

A large amount of work about interaction of highly charged ions with metal surface become interesting topics during the last 10 years (Hoffmann *et al.*, 2007; Zhang *et al.*, 2011; Xu *et al.*, 2012). When a highly charged ion impacts on a solid target, its potential energy is deposited within a few atomic layers and the kinetic energy is dissipated through electronic and nuclear stopping process (Schenkel *et al.*, 1998; Winter *et al.*, 1999). The inner-shell electrons of the target atoms are ionized and the vacancies decay either by Auger electrons emission or X-ray emission. Therefore, the investigation of the X-ray emission is useful method to study the mechanism of ion-solid collisions. Accurate measurement of the inner-shell ionization cross-section is essential for the development of ion-atom collision models and moreover significant to complete atomic data library for science research, in atomic physics, plasma physics, astrophysics, elemental analysis, biomedical research, environmental protection, and so on.

In a projectile ion and target collision, the target atom's inner-shell vacancies are created by direct ionization (DI), electron capture (EC), and electron promotion caused by molecular orbital (MO) formation. Direct ionization (Garcia *et al.*, 1970; Johnson *et al.*, 1979; Brandt *et al.*, 1981) plays an important role for $Z_1 < Z_2$ (Z_1 is the projectile atomic number and Z_2 is the target atomic number). Moreover, the relative velocity of projectile and target inner-shell electron is not important. Electron capture is the dominant mechanism for $Z_1 \leq Z_2$ and $v_1 \ll v_{2S}$ (v_1 is the projectile velocity and v_{2S} is the target inner-shell electron velocity). If projectiles with no K-shell vacancy, EC contribution can be negligible in target M-shell X-ray production cross-sections (Andrews *et al.*, 1987; Mehta *et al.*, 1983). For $Z_1 \approx Z_2$ and $v_1 \ll v_{2S}$, the molecular orbital model seems to be more suitable (Fano *et al.*, 1965).Various theoretical formulations are available for DI, such as the plane wave born approximation (PWBA) (Mukoyama, 1986), binary encounter approximation (BEA) (Gryzinski, 1965), and semiclassical approximation (Hansteen *et al.*, 1973). If relativistic effects (R), Coulomb deflection (C), and energy loss (E) become significant, the Heavy Ion Research Facility in Lanzhou (ECPSSR) (Brandt *et al.*, 1981; Lapicki *et al.*, 1980), which is based on the perturbed stationary state is the appropriate theoretical model. The Oppenheimer-Brinkman-Kramers model (Oppenheimer, 1928) accounts for EC from the target subshells to the projectile's unoccupied states.

Ionization studies and subsequent emission of the characteristic X-rays provide an insight into the processes involved in ion-atom collisions. Inner-shell ionization of atoms by charged particles and subsequent K- and L-shell X-ray production has been studied extensively (Soares *et al.*, 1976;

Address correspondence and reprint requests to: Yongtao Zhao, Insitute of Modern Physics. Chinese Academy of Science, Lanzhou, China. E-mail: zhaoyt@impcas.ac.cn

Mehta *et al.*, 1993; Awaya *et al.*, 1999; Szegedi *et al.*, 2001; Ouziane *et al.*, 2008; Zhang *et al.*, 2010). However, very little is known regarding the processes in Au M-shell. The ionization of M-shell can provide more information about the collision process because five subshells ($3s_{1/2}$, $3p_{1/2}$, $3p_{3/2}$, $3d_{3/2}$, and $3d_{5/2}$) are involved. Most of the previous work until now studied M-shell ionization with low Z projectiles (Rodríguez *et al.*, 2002; Singh *et al.*, 2006; Czarnota *et al.*, 2009) such as protons, helium ions, and other heavy ions (Be, C, O, and F). The limited data are achieved in heavy ions with several MeV energy. M-shell ionization phenomena are still a subject of investigation and are not yet fully understood. The comparison of the above-mentioned measurements with the theories indicates that the theoretical as well as the experimental understanding of the M-shell ionization by charged particles needs to be improved.

In this work, we present some recent experimental results on X-ray measurements originating from $^{36}Kr^{13+}$ ions beams impacting on an Au surface. The projectile initial kinetic energy ranged from 1.2 MeV to 3.6 MeV. Primary emphasis will be given to the investigation of projectile X-ray emission. The initial kinetic energy dependence of the X-ray yield will be discussed. Additionally target atom M X-ray production cross-section will be investigated in experiment and theory respectively.

2. EXPERIMENTAL SETUP

The experiment was performed on a 320 kV high voltage experimental platform at the Institute of Modern Physics, Chinese Academy of Science in Lanzhou. The experimental setup was shown in details in Zhao *et al.* (2009) and Zhang *et al.* (2011). The Kr with an incident angle of 45° to the surface, which was introduced into the ultrahigh vacuum target chamber (10^{-8} mbar) by deflection, focus and collimation, with spot size is about 5×5 mm, impacted perpendicularly onto the target surface. The emitted X-rays during ions-target collision were observed by silicon drift detector (XR-100SDD), which has a beryllium vacuum window in the front of the detector. Distance between the target and the detector is 32.5 cm. The detector has an energy resolution of about 136 eV at the energy of 5.899 keV and effective energy range of 0.8–100 keV. Efficiency calibration is given by the manufactory. A standard 55Fe source scales the X-ray detector before and after the measurement. The geometrical solid angle was about 0.0066 ± 0.00013 sr. The Au target had a purity of 99.99% with surface area of 15×20 mm^2 and thickness of 0.30 mm.

3. RESULTS AND DISCUSSION

3.1. Analysis of X-ray Spectra

Figure 1 shows the typical X-ray spectra induced by Krypton ions with 1.8–3.6 MeV impacting on Au target. The areas of X-ray peak were determined by Gauss fitting. Characteristic of X-ray a spectrum induced by Kr^{13+} with 1.8 MeV was shown in Figure 1a, two lines can be identified. The line at 1.637 keV has been identified as the characteristic L_α X-ray of Kr. The line at 2.169 keV has unambiguously

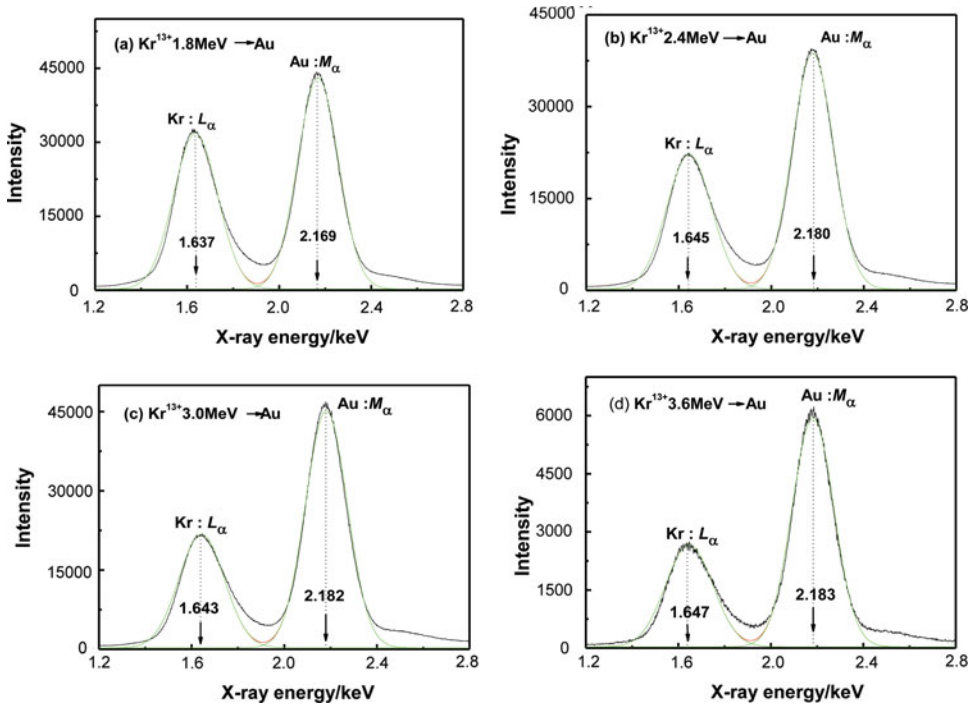

Fig. 1. (Color online) Characteristic of X-ray spectra induced by Kr^{13+} ions impacting on Au target.

https://doi.org/10.1017/S0263034612000638 Published online by Cambridge University Press

been identified as Au M_α radiation. So do this in Figures 1b, 1c, and 1d. Table 1 lists experimental energy of Kr L_α X-ray and Au M_α X-ray emission lines when Kr^{13+} with different energy impacts on an Au target. According to the (Thompson *et al.*, 2001) theoretical energy of Kr L_α X-ray and Au M_α X-ray emission line is 1.586 keV and 2.123 keV, respectively. In Table 1, compared to the *X-Ray Data Booklet*, we observed the experimental energy value of emission line is shifted 51–61 eV to higher energy, while Au M_α X-ray emission line has 46–60 eV energy shifting toward high energy. In addition, we list the full width at half maximum (FWHM) of the X-ray peak observed in the experiments. For Kr L_α X-ray line, the FWHM has a little growth tendency with the increasing of incident energy. For Au M_α X-ray line, the FWHM keeps almost constant in our energy range.

The initial electrons configuration Kr^{13+} is $1s^22s^22p^63s^23p^63d^5$, the binding energy of the 3d electrons is 93.8 eV. This is much lower than the binding energy of M-shell electrons for target atoms, which is 2206 eV (Thompson *et al.*, 2001). Because of the large mismatch between the projectile and target energy levels, electrons excitations are mainly caused by DI. Some works (Banaś *et al.*, 2002; Czarnota *et al.*, 2009) explain energy shifting by the multiple ionization effects, we estimated Kr L_α X-ray position by using energy difference between 3d and 2p orbital energy using the following formula (Li *et al.*, 1981):

$$(\overline{h\nu})_L = \bar{\varepsilon}_{3d} - \bar{\varepsilon}_{2p}, \tag{1}$$

where $\bar{\varepsilon}_{nl}$ is the inner-shell orbital energy, $\bar{\varepsilon}_{nl}$ can be given for a Rybderg-like equation.

$$\bar{\varepsilon}_{nl} = -\frac{(Z^*_{nl})^2}{2n^2}, \tag{2}$$

Where n is the principle quantum number, l is the azimuthal quantum number. $Z^*_{nl} = Z\text{-}\sigma_{nl}$ is effective nuclear charge. σ_{nl} is effective screening number in nl subshell from other electrons, which is always in connection with total electrons number but is independent of atomic number Z.

From above formula, we can get:

$$(\overline{h\nu})_L = \frac{5}{72}Z^2 - \frac{Z}{36}(9\sigma_2 - 4\sigma_3) + \frac{1}{72}(9\sigma_2^2 - 4\sigma_3^2), \tag{3}$$

where σ_2 and σ_3 are the effective shielding number in 2p and 3d subshell, respectively.

So, when ionization degree adds one degree, shift value of L_α X-ray can be given as:

$$\delta(\overline{h\nu})_L = \frac{Z}{36}(9\Delta\sigma_2 - 4\Delta\sigma_3) - \frac{1}{72}(18\sigma_2\Delta\sigma_2 - 9\Delta\sigma_2^2 - 8\sigma_3\Delta\sigma_3 + 4\Delta\sigma_3^2), \tag{4}$$

where $\Delta\sigma_2$ and $\Delta\sigma_3$ are reduction value of the effective screening number in 2p and 3d subshell, when reducing one electron in outer shell, respectively. In above formula, the second item is quadratic term, which value is small than the first item. When reducing one electron in the outer shell, $\Delta\sigma_2$ is bigger than $\Delta\sigma_3$, so $\delta(\overline{h\nu})_L > 0$. It means that the theoretical energy of Kr L_α X-ray is shifted to higher energy, which is the same with experimental value. Besides, we can also explain energy shifting of Au M_α X-ray emission line like Kr L_α X-ray.

3.2. X-ray Yield Per Ion

X-ray yield per incident particle is given by

$$Y(E) = \frac{N_x}{N_p\varepsilon(\Omega/4\pi)}, \tag{5}$$

where N_x is the number of observed X-ray counts that is extracted from the Gauss fitting of the spectrum by nonlinear curve fitting procedures. N_P is the total amounts of incident ions measured from target current corrected to the secondary electron emission. The true current can be estimated by $I = \frac{I_{\text{target}}}{1+\gamma/q}$ (Song *et al.*, 2011). Detection efficiency ε corresponding X-ray energy is 51% and 68% for Kr L_α and Au M_α X-ray, respectively. The solid angle of the detector Ω is 0.0066 sr.

The penetration depths are 0.20, 0.31, 0.42, 0.53, and 0.63 μm when Kr^{13+} ions impact on an Au target at the energies of 1.2, 1.8, 2.4, 3.0, and 3.6 MeV, respectively. Compared to the target thickness of 0.30 mm, the penetration depths is very small, therefore the target used in this work can be considered as a thick target.

The main uncertainty sources of the yield originated from the statistics of the X-ray counts about 5% and the

Table 1. *Characteristic of X-ray peak by Kr^{13+} ions impacting on Au target*

Incident Energy/MeV	Kr/L_α X-ray Peak (keV)		Au/M_α X-ray Peak(keV)	
	experimental energy	FWHM	experimental energy	FWHM
1.8	1.637	0.191 ± 0.005	2.169	0.178 ± 0.005
2.4	1.645	0.195 ± 0.005	2.180	0.179 ± 0.005
3.0	1.643	0.297 ± 0.005	2.182	0.181 ± 0.005
3.6	1.647	0.205 ± 0.005	2.183	0.181 ± 0.005

https://doi.org/10.1017/S0263034612000638 Published online by Cambridge University Press

measurement of the incident ions number about 10%. The total uncertainty of the yield was about 11% after the error propagation. The yield per ion of Au M_α X-ray and Kr L_α X-ray is shown in Figure 2.

As is shown in Figure 2, target atom M_α X-ray yield and projectile L_α X-ray yield scaled with incident energy was observed. The M_α X-ray of Au is unambiguous increasing with the incident energy increased. Compared to Au M_α X-ray yield, Kr L_α X-ray is increasing more slowly. Figure 3 shows the characteristic of X-ray spectra induced by Kr^{13+} ions impacting on Au target. We did not observe Kr K-shell X-ray.

In this work, for projectile, Kr L_α X-rays were determined only, which indicated that the 2p electrons of projectile were excited. With the incident energy increased, vacancies probability of occurrence in L-shell became bigger; therefore, Kr L_α X-ray yield is increased with increasing of incident energy. Since the initial electrons configuration of projectile Kr^{13+} is $1s^22s^22p^63s^23p^63d^5$, the M-shell electrons (such as 3s, 3p, 3d, and so on) will be easier excited than L-shell electrons. But M-shell holes de-excite corresponding energy is in visible light range, not in effective energy range of our detector. In addition, interaction energy between target and projectile is too small to excite Kr K-shell electrons. So Kr K-shell X-ray is not available. Au M_α X-ray yield is in close correlation with Au M_α X-ray production cross-section, we will talk it in next part.

3.3. M X-ray Production Cross-section

The X-ray production cross-section is derived from the X-ray yield using the standard formula for thick targets,

$$\sigma_x(E) = \frac{1}{N}\left[\frac{dY(E)}{dE}\cdot\frac{dE}{dR} + \frac{\cos\theta}{\cos\phi}\mu Y(E)\right], \tag{6}$$

where N is the target atom density (atoms/g), μ is the mass absorption coefficient of the target for its own characteristic X-rays given by McMaster (Grande *et al.*, 1970), θ is the incident angle to the normal direction of the target surface, ϕ is the observation angle to the target normal, $Y(E)$ is the single ion yield at projectile energy E, dY/dE is extracted from fitting polynomials to E and $Y(E)$, dE/dR is the stopping power that can be obtained by SRIM (http://www.srim.org).

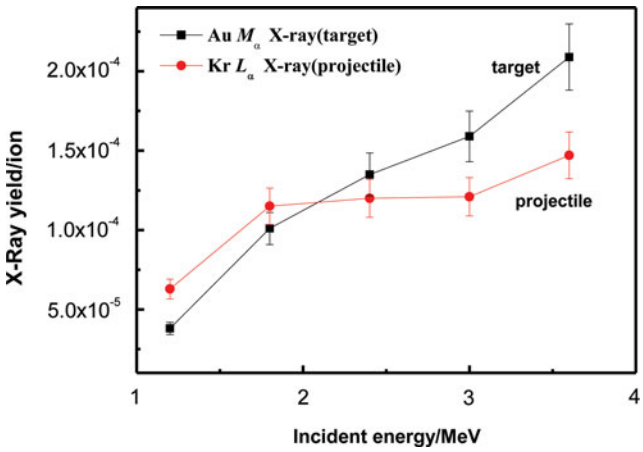

Fig. 2. (Color online) X-ray yields per ion *vs.* incident energy.

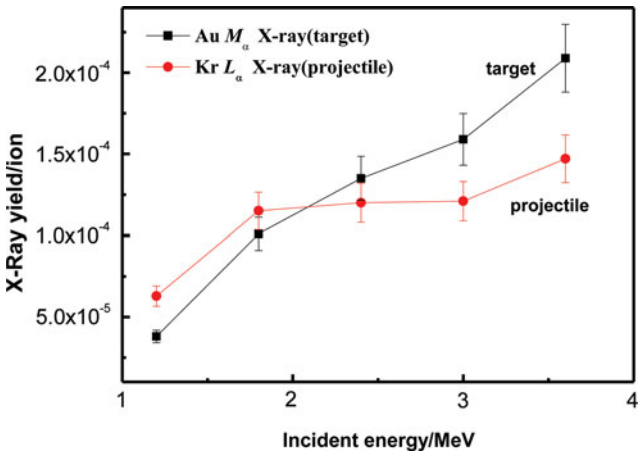

Fig. 3. (Color online) Characteristic of X-ray spectra induced by Kr^{13+} ions impacting on Au target.

In the following relations, the M X-ray production cross-section σ^X_{Mi} has been calculated from the theoretical M-subshell ionization cross-sections σ_{Mi} (based on the BEA theories) using atomic parameters such as the fluorescence yields (ω_i), Coster-Kronig transition factors (f_{ij}) and the super-Coster-Kronig factors (s_{ij}) from the works of McGuire (1972).

The X-ray production cross-sections are calculated from ionization cross-section as follows:

$$\begin{aligned}\sigma^X_{M_5}/\omega_5 = {} & \sigma_{M_5} + f_{45}\sigma_{M4} + (s_{35} + s_{34}f_{45})\sigma_{M3} \\ & + (s_{25} + s_{23}s_{35} + s_{24}f_{45} + s_{23}s_{34}f_{45})\sigma_{M2} \\ & + (s_{15} + s_{12}s_{25} + s_{13}s_{35} + s_{14}f_{45} + s_{12}s_{23}s_{35} \\ & + s_{12}s_{24}f_{45} + s_{13}s_{34}f_{45} + s_{12}s_{23}s_{34}f_{45})\sigma_{M1}\end{aligned} \tag{7}$$

$$\begin{aligned}\sigma^X_{M4}/\omega_4 = {} & \sigma_{M_4} + s_{34}\sigma_{M3} + (s_{24} + s_{23}s_{34})\sigma_{M2} + (s_{14} \\ & + s_{12}s_{24} + s_{13}s_{34} + s_{12}s_{23}s_{34})\sigma_{M1},\end{aligned} \tag{8}$$

$$\sigma^X_{M3}/\omega_3 = \sigma_{M3} + s_{23}\sigma_{M2} + (s_{13} + s_{12}s_{23})\sigma_{M1}, \tag{9}$$

$$\sigma^X_{M2}/\omega_2 = \sigma_{M2} + s_{12}\sigma_{M1}, \tag{10}$$

$$\sigma^X_{M1}/\omega_1 = \sigma_{M1}, \tag{11}$$

$$\sigma^X_M = \sum_{i=1}^{5}\sigma^X_{M_i}, \tag{12}$$

σ_{Mi} for the classical BEA prediction can be given in a close form as (Gryzinski, 1965),

$$\sigma^{BEA}_{Mi} = \left(\frac{NZ^2\sigma_0}{U^2}\right)G(V), \tag{13}$$

https://doi.org/10.1017/S0263034612000638 Published online by Cambridge University Press

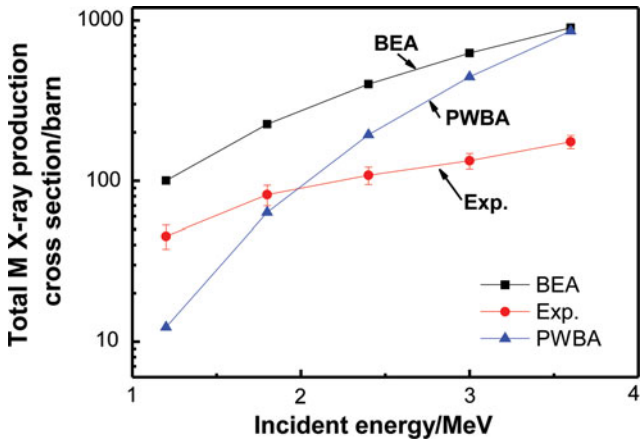

Fig. 4. (Color online) Total *M* X-ray production cross-sections of gold bombarded by 1.2–3.6 MeV krypton ions are shown for both experimental and theoretical results.

where N is the electron number for the I-shell, Z is the projectile nuclear charge, $\sigma_0 = \pi e^4 = 6.56 \times 10^{-14}$ cm^{2}eV^2; U is the electron binding energy, $G(V)$ is a universal function of the scaled velocity $V = v\,p/v\,i$ ($v\,p$ is the velocity of the projectile, $v\,i$ is the average velocity of the i-shell electron). In this work, for $V < 0.206$, $G(V)$ is approximately given by $4V^4/15$. Moreover, σ_i with the PWBA was calculated by a program developed by Liu *et al.* (1996).

We compared our experimental results to the BEA and PWBA models. The PWBA theoretical predictions are calculated with the version ADDS_v4_0 of program ISICS and the BEA theoretical predictions are calculated based on the above formulas. The results are shown in Figure 4.

All results of the M-shell X-ray production cross-sections of Au increased with increasing of the incident energy, which in accordance with the target X-ray yield. Most of the PWBA and BEA theoretical results are greater than the experimental value.

The classical BEA model is suitable for computing cross-section for the ionization of atoms by the impact of protons or other fully stripped nuclei. In this work, the projectile Kr^{13+} is not bare nucleus, therefore, the projectile nuclear Z_1 should be replaced by the effective nuclear charge Z_{eff} in the classical BEA formula. According to the initial electrons configuration of projectile Kr^{13+}, the value of Z_{eff} was taken approximately as 20 according to (http://en.wikipedia.org/wiki/Effective_nuclear_charge), taking the shielding effect of the orbital electrons into account. So the results from BEA model are bigger than that from experiments. In theoretical calculation, charge of projectile as a constant no matter incident energy it has. But in actual experiment, effective charge of projectile will change when the incident energy is different.

4. CONCLUSION

In this work, X-ray emission from $^{36}Kr^{13+}$ ions beams with 1.2–3.6 MeV impacting on an Au surface was measured. A shift of the X-ray lines to the higher energy side and line broadened were measured when incident energy increased. We also illustrated energy shifting range of Kr L_α X-ray line in theory. In addition, both the projectile and target atoms X-ray yield per incident particle were calculated, and both the two yields were increased with increasing of incident energy. Finally, Au M X-ray production cross-section were measured by experiments and calculated by both BEA and PWBA theoretical model respectively, besides, all the results were increased with increasing of incident energy.

ACKNOWLEDGMENTS

This work is supported by the Major State Basic Research Development Program of China ("973" program, Grant No. 2010CB832902) and the the National Natural Science Foundation of China (NSFC, Grant Nos.11075135, 11075192, 11075125).

REFERENCES

Andrews, M.C., Mcdaniel, F.D., Duggan, J.L., Miller, P.D., Pepmiller, P.L., Krause, H.F., Rosseel, T.M., Rayburn, L.A., Mehta, R. & Lapicki, G. (1987). L- and M-shell X-ray production cross-sections of Nd, Gd, Ho, Yb, Au, and Pb by 25-MeV carbon and 32-MeV oxygen ions. *Phys. Rev. A* **36**, 3699–3706.

Awaya, Y., Kambara, T. & Kanai, Y. (1999). Multiple K- and L-shell ionizations of target atoms by collisions with high-energy heavy ions. *Inter. J. Mass. Spec.* **192**, 49–63.

Banaś, D., Pajek, M., Semaniak, J., Braziewicz, J., Kubala-Kukuś, A., Majewska, U., Czyśewski, T., Jaskóla, M., Kretschmer, W., Mukoyama, T. & Trautmann, D. (2002). Multiple ionization effects in low-resolution X-ray spectra induced by energy heavy ions. *Nucl. Instr. Meth. Phys. Res. Sec. B* **195**, 233–246.

Brandt, W. & Lapicki, G. (1981). Energy-loss effect in inner-shell Coulomb ionization by heavy charged particles. *Phys. Rev. A* **23**, 1717–1729.

Czarnota, M., Banaś, D., Braziewicz, J., Semaniak, J. Pajek, M., Jaskola, M., Korman, A., Trautmann, D., Kretschmer, W., Lapicki, G., & Mukoyama, T. (2009). X-ray study of M-shell ionization of heavy atoms by 8.0–35.2-MeV O^{q+} ions: The role of the multiple ionization effects. *Phys. Rev. A* **79**, 032710.

Fano, U. & Lichten, W. (1965). Interpretation of Ar^+-Ar Collisions at 50 KeV. *Phys. Rev. Lett.* **14**, 627–629.

Garcia, J.D. (1970). Inner-shell ionizations by proton impact. *Phys. Rev. A* **1**, 280–285.

Grande, W.H.N.K.D., Mallett, J.H. & Hubbell, J.H. (1970). Compilation of X-ray cross-sections. Lawrence Livermore National Laboratory Report UCRL-50174 (Section I, 1970; Section II, 1969; Section III, 1969; Section IV, 1969).

Gryzinski, M. (1965). Classical theory of atomic collisions. I. Theory of inelastic collisions. *Phys. Rev. A* **138**, 336–358.

Hansteen, J.M. & Mosebekk, O.P. (1973). Atomic coulomb excitation by heavy charged particles. *Nucl. Phys. A* **201**, 541–560.

Hoffmann, D.H.H., Blazevic, A., Korostiy, S., Ni, P., Pikuz, S.A., Rosmej, O., Roth, M., Tahir, N.A., Udrea, S., Varentsov, D., Weyrich, K., Sharkov, B.Y. & Maron, Y. (2007). Inertial fusion energy issues of intense heavy ion and laser beams

https://doi.org/10.1017/S0263034612000638 Published online by Cambridge University Press

interacting with ionized matter studied at GSI-Darmstadt. *Nucl. Instr. Meth. Phys. Res. Sec. A* **577**, 8–13.

Johnson, D.E., Basbas, G. & Mcdaniel, F.D. (1979). X-ray Emission induced by 1.2-3.6 MeV Kr^{13+} ions. *At. Data Nucl. Data Tables* **24**, 1.

Lapicki, G., Laubert, R. & Brandt, W. (1980). Coulomb-deflection effect in inner-shell ionization by heavy charged particles. *Phys. Rev. A* **22**, 1889–1895.

Li, J.M. & Zhao, Z.X. (1981). Systematic variation of line-shift of K_α radiation from atomic ions. *Acta Phys. Sinica* **30**, 105–110.

Liu, Z.Q. & Cipolla, S.J. (1996). ISICS: A program for calculating K-, L- and M-shell cross-section from ECPSSR theory using a personal computer. *Comp. Phys. Communi.* **97**, 315–330.

McGuire, E.J. (1972). Atomic M-shell Coster-Kronig, auger, and radiative rates, and fluorescence yields for Ca-Th. *Phys. Rev. A* **5**, 1043–1047.

Mehta, R., Duggan, J.L., Mcdaniel, F.D., Andrews, M.C., Lapicki, G., Miller, P.D., Rayburn, L.A. & Zander, A.R. (1983). Direct ionization and electron capture in M-shell x-ray production by fluorine ions. *Phys. Rev. A* **28**, 2722–2726.

Mehta, R., Duggan, J.L., Mcdaniel, F.D., Mcneir, M.R., Yu, Y.C., Marble, D.K. & Lapicki, G. (1993). L-shell X-ray production cross-sections for 29Cu, 31Ga, 32Ge, 35Br, 39Y, 60Nd, 64Gd, 67Ho, 70Yb, 79Au, and 82Pb for 2-25 MeV carbon ions. *Nucl. Instr. Meth. Phys. Res. B* **79** 175–178.

Mukoyama, T. (1986). Relativistic calculations of the excitation cross-sections of hydrogen-like ions by heavy charged-particle impact. *Bull. Inst. Chem. Res.* **64**, 12–19.

Oppenheimer, J.R. (1928). On the quantum theory of the capture of electrons. *Phys. Rev.* **31**, 349–356.

Ouziane, S., Amokrane, A. & Toumert, I. (2008). Light ion induced L X-ray production cross-sections in Au and Pb. *Nucl. Instr. Meth. Phys. Res. B* **266**, 1209–1211.

Rodríguez-Fernández, L., Miranda, J., Ruvalcaba-Sil, J.L. Segundo, E. & Oliver, A. (2002). Measurement of M-shell X-ray production induced by protons of 0.3–0.7 MeV on W, Au, Pb, Bi, Th and U. *Nucl. Instr. Meth. Phys. Res. B* **189**, 27–32.

Schenkel, T., Hamza, A.V., Barnes, A.V., Schneider, D.H., Banks, J.C. & Doyle, B.L. (1998). Ablation of GaAs by intense, ultrafast electronic excitation from highly charged ions. *Phys. Rev. Lett.* **81**, 2590–2593.

Singh, Y.P., Misra, D., Kadhane, U. & Tribedi, L.C. (2006). Line-resolved M-shell X-ray production cross-sections of Pb and Bi induced by highly charged C and F ions. *Phys. Rev. A* **73**, 032712.

Soares, C.G., Lear, R.D., Lear, J.T., Sanders, J.T. & Van Rinsvelt, H.A. (1976). K-shell X-ray production cross-section for 1.0–4.4-MeV particles on selected thin targets of Z = 22–34. *Phys. Rev. A* **13**, 953–957.

Song, Z.Y., Yang, Z.H., Xiao, G.Q., Xu, G.Q., Chen, J. & Yang, Z.R. (2011). Charge state effect on K-shell ionization of aluminum by 600–3400 keV $xenon^{q+}$ ($12 < q < 29$) ion collisions. *Eur. Phys. J. D* **64**, 197–201.

Szegedi, S. & Fayez-Hassan, M. (2001). K X-ray production cross-sections for 40–180 keV protons. 3rd Conference on Nuclear & Particle Physics (NUPPAC'01) 20–24 October, Cairo, Egypt.

Thompson, A.C., Attwood, D.T., Gullikson, E.M., Howells, M.R., Kortright, J.B., Robinson, A.L. & Underwood, J.H. (2001). *X-ray Data Book*. Berkley: Lawrence Berkeley National Laboratory.

Winter, H.P., Eder, H. & Aumayr, F. (1999). Kinetic electron emission in the near-threshold region studied for different projectile charges. *Internat. J. Mass. Spectr.* **192**, 407–413.

Xu, Z.F., Zeng, L.X., Zhao, Y.T., Wang, J.G., Zhang, X.A., Xiao, G.Q. & Li, F.L. (2012). Charge effect in secondary electron emission from silicon surface induced by slow neon ions. *Laser Part. Beams* **30**, 319–324.

Zhang, H., Chen, X., Yang, Z., Xu, J., Cui, Y., Shao, J., Zhang, X., Zhao, Y., Zhang, Y. & Xiao, G. (2010). Molybdenum L-shell X-ray production by 350–600 keV Xe^{q+} ($q = 25$–30) ions. *Nucl. Instr. Meth. Phys. Res. B* **268**, 1564–1567.

Zhang, X.A., Zhao, Y.T., Hoffmann, D.H.H., Yang, Z.H., Chen, X.M., Xu, Z.F., Li, F.L. & Xiao, G.Q. (2011). X-ray emission of Xe^{30+} ion beam impacting on Au target. *Laser Part. Beams* **29**, 265–268.

Zhao, Y.T., Xiao, G.Q., Xu, H.S., Zhao, H.W., Xia, J.W., Jin, G.M., Ma, X.W., Liu, Y., Yang, Z.H., Zhang, P.M., Wang, Y.Y., Li, D.H., Zhao, H.Y., Zhan, W.L., Xu, Z.F., Zhao, D., Li, F.L. & Chen, X.M. (2009). An outlook of heavy ion driven plasma research at IMP-Lanzhou. *Nucl. Instr. Meth. Phys. Res. Sec. B* **267**, 163–166.